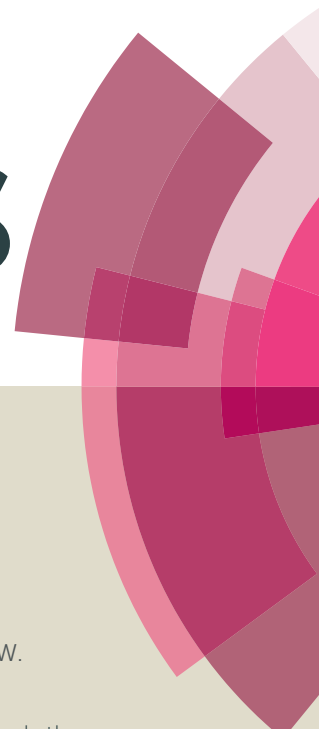


RSC Advances



This article can be cited before page numbers have been issued, to do this please use: Z. Zhang, J. Li, W. Gao, Z. Xia, Y. Qin, Y. Qu and Y. Ma, *RSC Adv.*, 2016, DOI: 10.1039/C6RA05967H.



This is an *Accepted Manuscript*, which has been through the Royal Society of Chemistry peer review process and has been accepted for publication.

Accepted Manuscripts are published online shortly after acceptance, before technical editing, formatting and proof reading. Using this free service, authors can make their results available to the community, in citable form, before we publish the edited article. This *Accepted Manuscript* will be replaced by the edited, formatted and paginated article as soon as this is available.

You can find more information about *Accepted Manuscripts* in the [Information for Authors](#).

Please note that technical editing may introduce minor changes to the text and/or graphics, which may alter content. The journal's standard [Terms & Conditions](#) and the [Ethical guidelines](#) still apply. In no event shall the Royal Society of Chemistry be held responsible for any errors or omissions in this *Accepted Manuscript* or any consequences arising from the use of any information it contains.



Thermally stable sandwich-type catalysts of Pt nanoparticles encapsulated in CeO₂ nanorods/CeO₂ nanoparticles core/shell supports for methane oxidation at high temperatures

Zhiyun Zhang, † Jing Li, † Wei Gao, Zhaoming Xia, Yuanbin Qin, Yongquan Qu, Yuanyuan Ma*

Received 00th January 20xx,
Accepted 00th January 20xx

DOI: 10.1039/x0xx00000x

www.rsc.org/

Thermal stability of nanocatalysts is of great importance to develop highly performed catalysts in terms of high activity and robust catalytic stability, especially for high-temperature catalysis. Herein, we report a sandwich-type Pt nanocatalyst encapsulated ceria-based core/shell supports (CNR@Pt@CNP), which consists of CeO₂ nanorod as core, CeO₂ nanoparticles as shell and Pt nanoparticles (PtNPs) embedded between CeO₂ nanorod and CeO₂ nanoparticles. The catalysts exhibited remarkable thermal stability at high temperature by effectively preventing PtNPs from thermal sintering. Methane combustion was carried out on the CNR@Pt@CNP catalysts at 400–700 °C to evaluate their catalytic activity and stability. With comparison to the same amount of PtNPs supported on CeO₂ nanorods (CNR@Pt), CNR@Pt@CNP delivered higher catalytic activity at high temperatures (>500 °C). The methane conversion catalyzed by CNR@Pt@CNP was slightly decreased from 82.3 % to 80.0 % after 12 hours at 650 °C. The improved performance of CNR@Pt@CNP originated from the CeO₂ nanoparticle as stabilizer, which can prevent the thermal sintering of PtNPs, strengthen the thermal stability of the catalysts and enhance the metal-support interaction.

Introduction

Nano-sized particles have attracted special attentions in heterogeneous catalysis due to their unique chemical and physical properties.^{1–3} The morphology, size, composition and spatial configuration of nanoscaled catalysts show capability to determine the catalytic activity and selectivity.^{3–5} Generally, a heterogeneous catalyst is comprised of two closely integrated parts: nanoscaled catalytic active component to activate the reactants and supports to facilitate the desired reactions, immobilize the nano-sized catalysts and maintain their dispersion on supports under the realistic conditions.⁶ However, an inherent challenge for nano-sized catalysts is to maintain their catalytic stability at the realistic operation conditions, especially for those catalytic reactions happened under the high temperatures.^{1, 2, 7–10} It is well known that the melting point of the nano-sized catalysts is significantly reduced due to the quantum confinement effect compared to their bulk counterpart, leading to a serious sintering and agglomeration of metallic

nanoparticles on supports at high temperatures.^{11, 12} The morphological features of nanocatalysts with well-defined shapes are also eliminated due to the thermal melting at high temperatures. Therefore, activity and selectivity of nanosized catalysts are significantly decreased for many high temperature catalytic processes including petroleum refining, Fischer-Tropsch synthesis of hydrocarbon fuels and automobile exhaust treatments.^{1, 13, 14} Besides the stability of active components, the stability of supports is also critical for activity and stability of the catalytic reactions. The chemically etched supports cannot host the nanocatalysts, leading to loss of the interaction between nano-sized catalysts and supports. The thermally collapsed supports shield the active sites and deny the accessibility of reactants to the catalytic centers.^{2, 7, 15} Therefore, the development of efficient and widely applicable strategies to stabilize nanocatalysts and their supports is highly desirable.

Recently, many strategies have been designed to increase the catalytic stability of metal nanocatalysts, such as sacrificial self-stabilization of metal nanocatalysts via alloying and encapsulation of nanocatalysts with metal oxide protection shell.^{1, 16–22} Core-shell configuration is commonly employed for stabilizing the heterogeneous catalysts, since their unique structure can avoid the aggregation of nano-sized catalysts in aqueous solution and prevent the nanocatalysts from sintering at elevated temperatures.^{23, 24} Besides, the specific interaction between core (nanocatalysts) and shell (supports) may improve the catalytic activity of metal nanocatalysts.²⁵ Silica has been

Center for Applied Chemical Research, Frontier Institute of Science and Technology, and State Key Laboratory for Mechanical Behavior of Materials, Xi'an Jiaotong University, Xi'an, China, 710049. E-mail: yyma@mail.xjtu.edu.cn

† Z. Zhang and J. Li give equally contribution.

Electronic Supplementary Information (ESI) available: [The XPS survey spectra of the catalysts. The XRD patterns of the spent CNR@Pt and CNR@Pt@CNP catalysts after reaction and the XRD patterns of catalysts after calcination at 400 °C, 500 °C and 700 °C. TGA profiles of fresh CNR@Pt and CNR@Pt@CNP catalysts.].

See DOI: 10.1039/x0xx00000x

widely used as the "stabilizer" of metal nanocatalysts because of its good thermal stability and tolerance towards acidic media.^{24, 26} Pt nanoparticles encapsulated in mesoporous silica exhibited a significantly enhanced thermal stability up to 750 °C.¹⁸ Recently, a sandwich-type Pt core@shell catalyst (SiO₂@Pt@SiO₂) showed the ability against sintering of the nanoparticles up to 500 °C for n-hexane reforming.²³

Ceria is widely explored as supports, promoters and active components in a wide range of applications such as three-way catalysts, oxygen sensors and solid fuel cells.^{21, 27} Moreover, ceria with the reversible transformation between Ce³⁺ and Ce⁴⁺ shows excellent capacity to stabilize the metal nanocatalysts due to the strong metal-support interface interaction and effective capability to resist the coke formation originated from its high oxygen mobility.^{4, 28, 29} Pt/CeO₂ catalysts are considered as the most effective catalysts in automotive exhaust abatement, water gas shift reaction and methane oxidation.^{15, 30, 31} However, Pt/CeO₂ catalysts usually lose their activity at high temperature due to the thermal sintering of PtNPs.

Herein, a sandwich-type ceria-based core-shell catalyst with encapsulated PtNPs (CNR@Pt@CNP), composed of CeO₂ nanorod core as the supports, thin CeO₂ nanoparticles shell as the stabilizer and PtNPs embedded as the nanocatalysts, exhibited remarkable thermal stability, high catalytic activity and robust catalytic activity for methane combustion. The catalyst is synthesized through the facile wet chemistry. The superior performance of CNR@Pt@CNP catalysts for methane combustion is attributed to the presence of thin CeO₂ nanoparticle shell as the stabilizer.

Experimental Section

Synthesis of CeO₂ Nanorods

For a typical synthesis, 1.736 g of Ce(NO₃)₃·6H₂O was dissolved in 10 mL of Milli-Q water (18.2 MΩ·cm), and 19.2 g of NaOH was dissolved in 70 mL of MQ water. After aging of the mixed solution of Ce(NO₃)₃·6H₂O and NaOH for 30 min, the mixture was transferred into a stainless steel autoclave for hydrothermal treatment at 100 °C for 24 h. The products were centrifuged off, washed by copious amount of MQ water and dried at 60 °C overnight.

Modification of CeO₂ Nanorods by Aminopropyltriethoxysilane (APTES)

To functionalize the surface of CeO₂ nanorods with amino groups, 1.0 g of CeO₂ nanorods was dispersed in 100 mL of ethanol *via* sonication. After addition of 1.0 mL of APTES, the solution was refluxed for 6 h under the continuous stirring. The modified CeO₂ nanorods were collected by centrifugation followed by thorough washing with ethanol for three times. The APTES-functionalized CeO₂ nanorods were dispersed in 100 mL of water with a concentration of 10 mg/mL for future use.

Synthesis of Pt Nanoparticles

PtNPs were synthesized by refluxing a mixed solution containing 6.65 mg of polyvinylpyrrolidone (PVP, MW=55,000), 31.08 mg of H₂PtCl₆·6H₂O, 10 mL of MQ water

and 90 mL methanol for 3 h. Then, 10 mL of 6.0 mM H₂PtCl₆·6H₂O aqueous solution and 90 mL of methanol were added into the above solution. Finally, the mixture was refluxed for another 3 h.

Synthesis of CeO₂ Nanorods Decorated with PtNPs (CNR@Pt)

To anchor PtNPs onto the surface of CeO₂ nanorods, 26.4 mL of as-synthesized PtNPs solution mixed with 10 mL of the stock suspension of CeO₂ nanorods modified by APTES. After stirring continuously at room temperature for 3 h, the resulted products, CNR@Pt, were separated by centrifugation and washed with water for three times. Finally, the catalysts were dried at 60 °C and calcined at 400 °C for 4 h.

Synthesis of CNR@Pt@CNP Catalysts

The CNR@Pt catalysts were then re-dispersed in a cetyltrimethyl ammonium bromide (CTAB) aqueous solution (0.025 M) with a concentration of 10 mg/mL. For chemical deposition of thin CeO₂ nanoparticle shell, 40 mL of 10 mM ethylene diamine tetraacetic acid (EDTA) aqueous solution, 4 mL of 0.1 M Ce(NO₃)₃ aqueous solution and 40 μL of the concentrated ammonia solution were added into 5 mL of the stock CNR@Pt solution sequentially. After sonication for 30 min, the mixture was stirred at 90 °C for 3 h. The sandwich-type CNR@Pt@CNP catalysts were collected by centrifugation, washed with MQ water for three times, dried at 60 °C overnight and then calcined at 400 °C for 4 h.

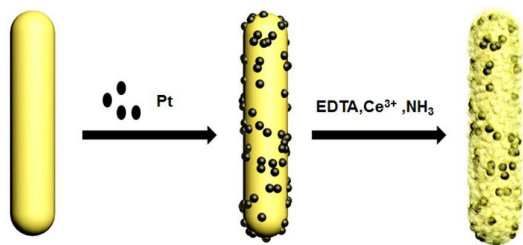
Characterization

Transmission electron microscopy (TEM) was conducted on a Hitachi HT7700 microscopy at an accelerating voltage of 120 kV. High resolution and dark field TEM images were performed on an FEI Tecnai G2 F20 S-Twin microscope with the accelerating voltage of 200 kV. X-ray diffraction (XRD) measurements of the catalysts were obtained on a PW 1710 Philips Powder X-ray diffractometer. The Pt content was determined by inductively coupled plasma optical emission spectroscopy (ICP-OES) analysis. X-ray photoelectron spectra (XPS) of catalysts were acquired on a Thermo Electron Model K-Alpha with Al K α as the excitation source. The specific surface area was calculated by the Brunauer-Emmett-Teller (BET) method. Thermogravimetry analyses (TGA) of the fresh samples were performed in the range 30–800 °C using a Netzsch STA449C thermoanalyzer with a heating rate of 10 °C min⁻¹ under static air. H₂ temperature-programmed reduction (H₂-TPR) was carried out in a ChemBET TPR/TPD3000 apparatus. In each run, 100 mg of catalyst was pretreated at 300 °C for 30 min in a flowing stream of high-purity argon (30 mL min⁻¹). After cooling to room temperature, a 5 % H₂ in Ar with a flow rate of 30 mL min⁻¹ was introduced and the programming temperature was controlled from room temperature to 850 °C with a ramping rate of 10 °C min⁻¹.

Catalytic Reaction

The methane combustion was carried out in a fixed-bed quartz reactor with an inner diameter of 4 mm at the atmospheric pressure. CH₄ (1 vol %) and air (99 vol %) were fed by mass flow controllers at a space velocity of 240,000 mL h⁻¹ g⁻¹_{cat}.

Journal Name



Scheme 1. Preparation process of the sandwich-type Pt encapsulated ceria-based core-shell catalysts (CNR@Pt@CNP).

The catalytic reactions were carried out from 300 °C to 700 °C with a ramping rate of 5 °C min⁻¹. At each temperature, the reaction efficiency was recorded after 30 min of steady-state. Process gas was analyzed by gas chromatography (GC) equipped with flame ionization detector (FID, Porapark-Q column). Catalytic stability of catalysts was evaluated at 650 °C.

Results and Discussion

Synthesis and Characterization of the Sandwich-Type CNR@Pt@CNP Catalysts

As illustrated in Scheme 1, synthesis of the sandwich-type core@shell CNR@Pt@CNP catalysts involves three steps: (1) hydrothermal synthesis of CeO₂ nanorods followed by the surface functionalization of APTES; (2) conjugation of pre-synthesized PtNPs onto the surface of CeO₂ nanorods *via* electrostatic force; and (3) chemical deposition of thin CeO₂ nanoparticle shell as stabilizer by a slow hydrolysis of cerium (III)-EDTA complex precursor.

CeO₂ nanorods were synthesized by hydrothermal process at 100 °C for 24 h, as described in previous reports.³²⁻³⁴ TEM image (Fig. 1a) shows a rod-like morphology with a diameter of 13 ± 3.2 nm and a length of 135 ± 38 nm. XRD pattern of CeO₂ nanorods confirms the cubic fluorite phase (Fig. 1i, JCPDS No. 75-0076) of as-synthesized nanostructures. PtNPs were synthesized by chemical reduction of H₂PtCl₆ by methanol.^{35,36} The average size of PtNPs is 4.1 ± 0.7 nm (Fig. 1b). The bright field TEM image (Fig. 1c) indicates the successful formation of CNR@Pt catalysts through the electrostatic force between the negatively charged PtNPs and the positively charged CeO₂ nanorods modified with amino groups under the reaction conditions.²⁵ The dark field TEM image (Fig. 1d) further confirms the conjugation between CeO₂ nanorods and PtNPs. The size of PtNPs in CNR@Pt catalysts is 4.0 ± 0.9 nm, which is in consistent with the size of as-synthesized PtNPs. The high resolution TEM (HRTEM, Fig. 1e) study on CNR@Pt catalysts shows that both CeO₂ nanorods and PtNPs exhibit a good crystallinity. A fringe distance of 0.22 nm is observed for the anchored PtNPs, which corresponds to the (111) crystalline plane of Pt metal. The existence of metallic Pt phase in CNR@Pt catalysts is further revealed from XRD pattern (Fig. 1i) of CNR@Pt, in which a weak peak at 39.8 ° corresponds to the (211) Bragg reflection of the metallic Pt phase (Fig. 1i). The derived size of PtNPs from XRD profile

by Scherrer-Warren equation is 5.14 nm, which is consistent with that observed in TEM. The measured surface area of CNR@Pt catalysts is 94.3 m²/g. ICP-OES analysis indicates the actual Pt loading in CNR@Pt is 2.18 wt%.

A surfactant templating method was used to grow thin CeO₂ nanoparticle shell on the surface of CNR@Pt.³⁷ The formation of Ce(III)-EDTA complex ions is critical for the slow hydrolysis of cerium precursor in basic solution. At 90 °C, the Ce(III)-EDTA precursor hydrolyzed slowly and deposited preferentially on the surface of CNR@Pt catalysts. Accompanied by the oxidation of the hydrolyzed cerium species by dissolved O₂ in reaction solution, the CNR@Pt@CNP catalysts are obtained by the formation of the thin CeO₂ nanoparticle shell as the stabilizer for the embedded PtNPs. Both bright field and dark field TEM images (Fig. 1f and 1g) demonstrate the sandwich-like structural features of the CNR@Pt@CNP catalysts, in which PtNPs are anchored on the surface of CeO₂ nanorods and the majority of PtNPs are surrounded by the small ceria nanoparticles with a size of 2.2 ± 0.2 nm. No free ceria nanoparticles are observed, indicating that the nucleation and subsequent growth of the ceria stabilizer indeed happen on the surface of CNR@Pt. From dark field TEM image (Fig. 1g), the average size of the embedded PtNPs is 4.1 ± 0.6 nm, consistent with that of as-synthesized PtNPs. HRTEM image of the CNR@Pt@CNP catalysts (Fig. 1h) reveals a lattice spacing of 0.22 nm, suggesting the high crystallinity and well maintained metallic phase of PtNPs during the chemical deposition of ceria stabilizer. XRD pattern

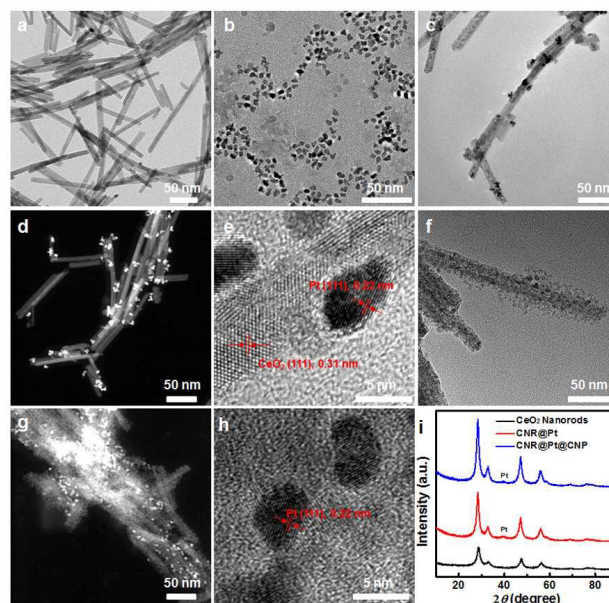


Fig. 1. Structural characterization of catalysts. (a) TEM image of CeO₂ nanorods, (b) TEM image of PtNPs, (c) Bright field TEM image of the CNR@Pt catalysts. (d) Dark field TEM image of the CNR@Pt catalysts. (e) HRTEM image of the CNR@Pt catalysts. (f) Bright field TEM image of the CNR@Pt@CNP catalysts. (g) Dark field TEM image of the CNR@Pt@CNP catalysts. (h) HRTEM image of the CNR@Pt@CNP catalysts. (i) XRD patterns of the CeO₂ nanorods, CNR@Pt catalysts and the CNR@Pt@CNP catalysts.

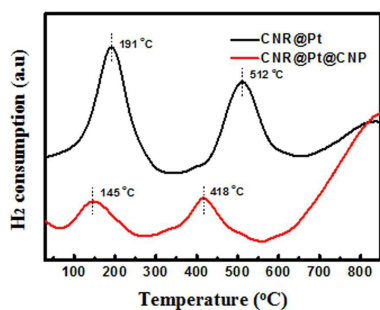


Fig. 2. H₂-TPR profiles of the CNR@Pt and CNR@Pt@CNP catalysts.

of the CNR@Pt@CNP catalysts (Fig. 1i) further confirms the coexistence of the CeO₂ cubic fluorite phase and metallic Pt phase, which is also verified by the XPS profile (Fig. S1). The calculated average size of PtNPs from XRD pattern for the CNR@Pt@CNP catalysts is 4.7 nm, similar to that in the CNR@Pt catalysts. The surface area of CNR@Pt@CNP catalysts is slightly decreased from 94.3 m²/g of the CNR@Pt catalysts to 78.5 m²/g. ICP analysis of the CNR@Pt@CNP catalysts indicates the weight percentage of Pt in the catalysts is 1.86 wt%.

Redox Properties and Thermal Stability of CNR@Pt and CNR@Pt@CNP Catalysts.

The redox properties of the CNR@Pt and CNR@Pt@CNP catalysts were studied by H₂-TPR in the temperature range from room temperature to 850 °C. H₂-TPR profiles of the CNR@Pt and CNR@Pt@CNP catalysts (Fig. 2) exhibit two distinct temperature peaks. The first peak at 191 °C for CNR@Pt and at 145 °C for CNR@Pt@CNP is attributed to the reduction of Pt oxides and surface active oxygen. The second peak located at 512 °C for CNR@Pt and at 418 °C for CNR@Pt@CNP corresponds to the reduction of lattice oxygen. Compared with the reduction peaks of CNR@Pt, the peak shift of CNR@Pt@CNP to lower temperatures indicates a stronger interaction between Pt and CeO₂ for the CNR@Pt@CNP catalysts.³⁸

Thermal stability of the CNR@Pt and CNR@Pt@CNP catalysts was evaluated by calcining as-synthesized catalysts at 400 °C, 500 °C and 700 °C under ambient conditions for 4 h, respectively. The morphological evolution of the catalysts and the size change of PtNPs were examined by TEM technique. As shown in Fig. 3, CNR@Pt@CNP catalysts exhibit a good thermal stability and the rod-like morphology is well preserved even at a high temperature of 700 °C. At 400 °C, the structural stability of both CNR@Pt and CNR@Pt@CNP catalysts is revealed from TEM images (Fig. 3a and 3b). The average sizes of PtNPs in CNR@Pt and CNR@Pt@CNP are 4.3 ± 0.9 nm and 4.2 ± 0.8 nm, respectively, which are very close to the values of as-synthesized catalysts. Increasing the temperature to 500 °C, PtNPs in CNR@Pt significantly aggregate with an average diameter of 10.1 ± 4.0 nm (Fig. 3c), indicating the melting, migration and aggregation of small PtNPs during the calcination. Bigger particles (>20 nm) are also observed. In contrast, the morphology of the CNR@Pt@CNP catalysts is well preserved. The small PtNPs with a slightly increased

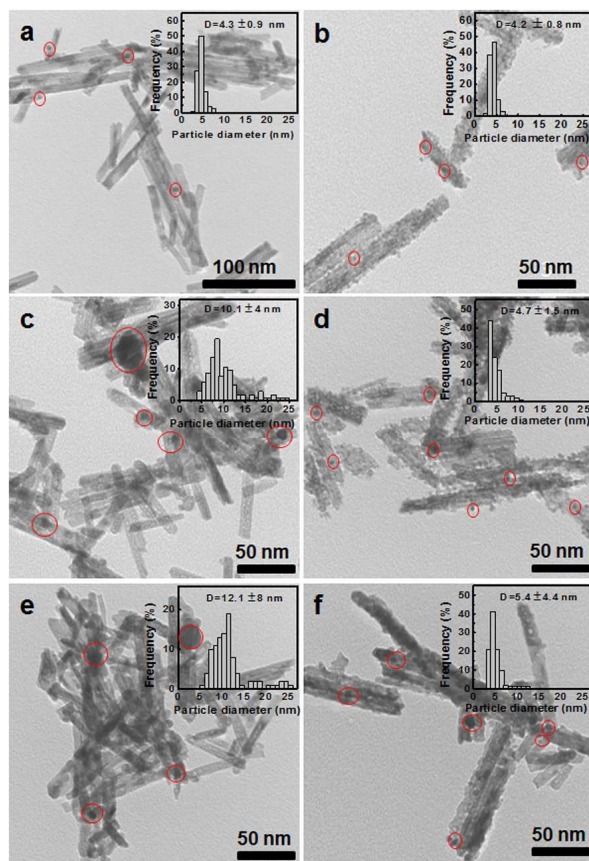


Fig. 3. Thermal stability of the CNR@Pt and CNR@Pt@CNP catalysts by annealing at various temperatures. (a) TEM characterization of CNR@Pt after calcination at 400 °C for 4h, (b) TEM characterization of CNR@Pt@CNP after calcination at 400 °C for 4h. (c) TEM characterization of CNR@Pt after calcination at 500 °C for 4h, (d) TEM characterization of CNR@Pt@CNP after calcination at 500 °C for 4h. (e) TEM characterization of CNR@Pt after calcination at 700 °C for 4h, (f) TEM characterization of CNR@Pt@CNP after calcination at 700 °C for 4h. Inset images showed the size distribution of PtNPs of the catalysts calcinated at various temperatures.

average diameter of 4.7 ± 1.5 nm are well encapsulated within CeO₂ nanoparticle shell. The results indicate that the CeO₂ nanoparticles serve as a physical barrier to prevent the migration and sintering of PtNPs. On the further calcinations at a high temperature of 700 °C, PtNPs merge into even larger particles of 12.1 ± 8.0 nm for the CNR@Pt catalysts (Fig. 3e). For the CNR@Pt@CNP catalysts, the small ceria nanoparticles tend to melt and result in a strong interaction with PtNPs and CeO₂ nanorods. The average diameter of PtNPs is 5.4 ± 4.4 nm and a few big metal nanoparticles (> 12.0 nm) are observed in Fig. 3f. This may be attributed to the melting of small ceria nanoparticles, which makes the merging of adjacent PtNPs become possible. However, the small PtNPs are the dominant metal particles in the CNR@Pt@CNP catalysts. In their XRD patterns (Fig. S3), the increased peak intensities of Pt for the CNR@Pt catalysts at the elevated temperatures further confirmed the thermal aggregation of Pt nanoparticles in CNR@Pt. In contrast, the similar peak intensities of Pt were observed for as-synthesized CNR@Pt@CNP and catalysts

Journal Name

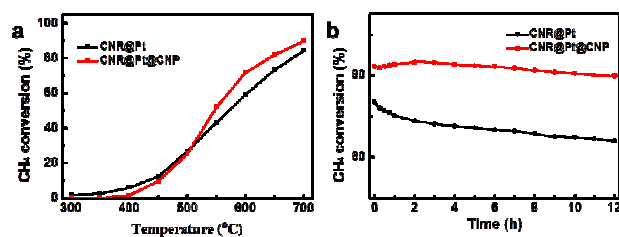


Fig. 4. (a) Methane conversion as a function of temperature in methane oxidation with CNR@Pt and CNR@Pt@CNP catalysts. (b) Stability of CNR@Pt and CNR@Pt@CNP catalysts for methane oxidation at 650 °C.

treated at 500 °C and 700 °C (Fig. S3). Thus, both TEM and XRD studies of the CNR@Pt and CNR@Pt@CNP catalysts after calcination at various high temperatures further confirm that the small CeO₂ nanoparticle shell as the stabilizer can effectively protect small PtNPs from the surface migration and aggregation into large ones.

Catalytic Performances

The described improvements in the thermal stability of PtNPs in the sandwich-type CNR@Pt@CNP structure have potential implications for high temperature reactions. The catalytic combustion of methane was employed as a model reaction to evaluate the catalytic activity and stability of PtNPs of the CNR@Pt@CNP catalysts at high temperatures. The CNR@Pt and CNR@Pt@CNP catalysts with 0.22 mg of PtNPs were used for the combustion of CH₄ (CH₄ + 2O₂ = CO₂ + 2H₂O). The TGA profiles of the CNR@Pt and CNR@Pt@CNP catalysts (Fig. S2) demonstrate that organic residuals during the synthetic process can be removed after treatment at 400 °C in air. Thus, the catalysts were calcinated in air for 4 h before the catalytic reactions. Fig. 4a presents the catalytic efficiency of two catalysts in terms of CH₄ conversion as a function of the reaction temperatures. The conversions of CH₄ are largely dependent on the reaction temperatures. Specifically, the increase of the reaction temperature results in the elevated conversion of CH₄. As shown in Fig. 4a, the methane conversions of CNR@Pt catalysts are increased from 2.1 % to 2.7 %, 6.1 %, 12.6 %, 26.8 %, 43.2 %, 59.3 %, 73.3 %, and 84.5 % for the reaction temperatures at 300 °C, 350 °C, 400 °C, 450 °C, 500 °C, 550 °C, 600 °C, 650 °C and 700 °C, respectively.

For the CNR@Pt@CNP catalysts, the methane conversions are lower than those of CNR@Pt, when the reaction temperature is below 500 °C. After that, the CNR@Pt@CNP catalysts deliver a higher catalytic activity than the CNR@Pt catalysts. This phenomenon can be attributed to the structure-activity correlation. At low temperatures, the partial surface area of PtNPs embedded in the sandwich-type CNR@Pt@CNP catalysts is blocked by ceria nanoparticles. Meanwhile, PtNPs either on CeO₂ nanorods or in the sandwich-type catalysts preserve their original size at low temperatures (Fig. 3a and 3b). Hence, more catalytic sites in CNR@Pt are exposed for the access of the reactants, resulting in a higher methane conversion catalyzed by the CNR@Pt catalysts. Increasing reaction temperatures, the size of PtNPs embedded in the

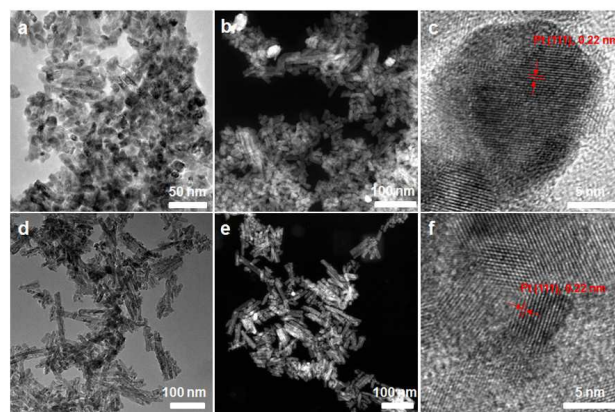


Fig. 5. TEM images of CNR@Pt and CNR@Pt@CNP catalysts for methane oxidation at 650 °C for 12h. (a) TEM image of CNR@Pt, (b) Dark field TEM image of CNR@Pt, (c) HRTEM image of CNR@Pt, (d) TEM image of CNR@Pt@CNP, (e) Dark field TEM image of CNR@Pt@CNP, (f) HRTEM image of CNR@Pt@CNP.

core/shell CeO₂ is only slightly increased, while small PtNPs anchored on the surface of CeO₂ nanorods in the absence of the ceria nanoparticle shell significantly aggregate into large ones. Consequently, the available active sites in the CNR@Pt@CNP catalysts surpass those in the CNR@Pt catalysts at high temperatures. This critical temperature point is observed at 500 °C. PtO_x is recognized as the active phase for this reaction.^{39, 40} Thus, the oxygen donation capability of ceria nanostructures also contributes to stabilize size of catalysts.^{39, 40} H₂-TPR profiles (Fig. 2) suggest the stronger metal (Pt)-support (CeO₂) interaction for the CNR@Pt@CNP catalysts, indicating their improved thermal stability and enhanced catalytic activity as a consequence.

The catalytic stability for both two catalysts was performed at 650 °C for 12 h of continuous reaction, in which the methane conversion was recorded as a function of the reaction time (Fig. 4b). The methane conversion with time on stream catalyzed by CNR@Pt catalysts was decreased from 73.3 % to 63.9 % after 12 h reaction. Especially, the methane conversion rapidly decreased from 73.3 % to 67.2 % during the first 5 h. In contrast, the methane conversions were slightly dropped from 82.3 % to 80.0 % for a period of 12 h, when the CNR@Pt@CNP catalysts were used as the catalysts. Such a difference in their catalytic stability can be unambiguously attributed to the stabilized PtNPs, which are protected by the ceria nanoparticle shell in the sandwich-type CNR@Pt@CNP catalysts.

To further illustrate the roles of ceria nanoparticle shell as the stabilizer for the PtNPs in the realistic catalytic conditions, the catalysts after 12 h reactions were characterized by TEM techniques. As shown in Fig. 5a-5c, PtNPs in the CNR@Pt catalysts sintered seriously after 12 h reaction at 650 °C. Small PtNPs are barely observed and large PtNPs (> 30 nm) are revealed from the dark-field TEM image (Fig. 5b). Of note, CeO₂ nanorods were also broken into short ones after a long period of continuous reactions. In contrast, the rod-like morphology of the CNR@Pt@CNP catalysts was well preserved after 12 h continuous reactions, despite very small

amount of broken pieces were also observed. Derived from both bright field and dark field TEM images (Fig. 5d-5f), the average size of PtNPs of the CNR@Pt@CNP catalysts is 5.9 ± 2.1 nm, which may explain the slightly decreased methane conversion. The results suggest that PtNPs in the CNR@Pt catalysts sinter into large particles (Fig. 5a-6c) and PtNPs in the CNR@Pt@CNP catalysts (Fig. 5d-5f) are still small. Size evolution of PtNPs also can be reflected from the XRD patterns of the spent catalysts (Fig. S4). After 12-hour reaction at 650 °C, the XRD peak of metallic Pt phase at 39.5 ° is still very weak for the CNR@Pt@CNP catalysts, similar to that of as-synthesized catalysts. While, the XRD peak of PtNPs for the spent CNR@Pt is much stronger than that of the fresh CNR@Pt catalysts. The results also suggest the aggregated PtNPs in the CNR@Pt catalysts and preserved small PtNPs in the CNR@Pt@CNP catalysts, which are consistent with the observations in TEM images. The sum of the above observations clearly indicate that the CeO₂ nanoparticle shell of CNR@Pt@CNP functions as the stabilizer provides a physical barrier to prevent PtNPs from sintering, and strengthens the metal-support interface interaction and thermal stability of the CeO₂ nanorod core. Thus, the remarkable thermal stability of CNR@Pt@CNP catalysts can provide more accessible active sites for catalytic reaction, leading to a stabilized activity at high temperatures. The thermal stability and catalytic activity of the CNR@Pt@CNP catalysts are comparable with or even better than those of similar Pt/CeO₂ core/shell catalysts for high temperature methane oxidation.^{17, 20, 22, 41-43}

Conclusions

The sandwich-type CNR@Pt@CNP catalysts, prepared via a facile wet chemical synthetic route, exhibited a high activity and stability for the methane oxidation at high temperatures. The high activity and stability of the CNR@Pt@CNP can be ascribed to their unique physical structure by providing a thin ceria nanoparticle shell to prevent PtNPs from sintering, strengthen the thermal stability of the core of CeO₂ nanorods and enhance the Pt-CeO₂ interaction. Hence, the sandwich-type CNR@Pt@CNP catalysts with good activity and stability may serve as potential catalysts for the catalytic processes at high temperature, especially for those involving hydrocarbon molecules.

Acknowledgements

We acknowledge the financial support from a NSFC Grant 21401148, the Ministry of Science and Technology of China through a 973-program under Grant 2012CB619401 and the Fundamental Research Funds for the Central Universities. Technical supports for TEM experiments from State Key Laboratory for Mechanical Behavior of Materials, Xi'an Jiaotong University, is also acknowledged.

References

1. A. Cao and G. Vesper, *Nat. Mater.*, 2010, **9**, 75-81.

2. A. Cao, R. Luc and G. t. Vesper, *Physical Chemistry Chemical Physics*, 2010, **12**, 13499-13510.
3. C. T. Campbell, S. C. Parker and D. E. Starr, *Science*, 2002, **298**, 811-814.
4. C. Aydin, J. Lu, N. D. Browning and B. C. Gates, *Angew. Chem. Int. Ed. Engl.*, 2012, **51**, 1-7.
5. Y. Chen, H. Chen, L. Guo, Q. He, F. Chen, J. Zhou, J. Feng and J. Shi, *ACS Nano*, 2010, **4**, 529-539.
6. J. Lu, J. W. Elam and P. C. Stair, *Acc. Chem. Res.*, 2013, **46**, 1806-1815.
7. J. Wang, A.-H. Lu, M. Li, W. Zhang, Y.-S. Chen, D.-X. Tian and W.-C. Li, *ACS Nano*, 2013, **7**, 4902-4910.
8. G. Prieto, M. Shakeri, K. P. d. Jong and P. E. d. Jongh, *ACS Nano*, 2014, **8**, 2522-2531.
9. X. Liu, A. Wang, X. Yan, T. Zhang, C.-Y. Mou, D.-S. Su and J. Li, *Chem. Mater.*, 2009, **21**, 410-418.
10. G. Prieto, J. Zečević, H. Friedrich, K. P. d. Jong and P. E. d. Jongh, *Nat. Mater.*, 2013, **12**, 34-39.
11. J. A. Farmer and C. T. Campbell, *Science*, 2010, **329**, 933-936.
12. X. Yan, X. Wang, Y. Tang, G. Ma, S. Zou, R. Li, X. Peng, S. Dai and J. Fan, *Chem. Mater.*, 2013, **25**, 1556-1563.
13. H. S. Gandhi, G. W. Graham and R. W. McCabe, *J. Catal.*, 2003, **216**, 433-442.
14. J. Lu, B. Fu, M. C. Kung, G. Xiao, J. W. Elam, H. H. Kung and P. C. Stair, *Science*, 2012, **335**, 1205-1208.
15. S. Damyanova, B. Pawelec, K. Arishtirova, M. V. M. Huerta and J. L. G. Fierro, *Appl. Catal., B*, 2009, **89**, 149-159.
16. M. Cargnello, N. L. Wieder, T. Montini, R. J. Gorte and P. Fornasiero, *J. Am. Chem. Soc.*, 2010, **132**, 1402-1409.
17. X. Wang, D. Liu, S. Song and H. Zhang, *J. Am. Chem. Soc.*, 2013, **135**, 15864-15872.
18. S. H. Joo, J. Y. Park, C.-K. Tsung, Y. Yamada, P. Yang and G. A. Somorjai, *Nat. Mater.*, 2009, **8**, 126-131.
19. Y. Chen, H. Chen, L. Guo, Q. He, F. Chen, J. Zhou, J. Feng and J. Shi, *ACS Nano*, 2010, **4**, 529-539.
20. S. Song, X. Wang and H. Zhang, *NPG Asia Materials*, 2015, **7**, e179.
21. G. Chen, F. Rosei and D. Ma, *Nanoscale*, 2015, **7**, 5578-5591.
22. K. Yoon, Y. Yang, P. Lu, D. Wan, H.-C. Peng, K. S. Masias, P. T. Fanson, C. T. Campbell and Y. Xia, *Angew. Chem. Int. Ed. Engl.*, 2012, **51**, 9543-9546.
23. K. An, Q. Zhang, S. Alayoglu, N. Musselwhite, J.-Y. Shin and G. A. Somorjai, *Nano Letters*, 2014, **14**, 4907-4912.
24. J. C. Park, J. U. Bang, J. Lee, C. H. Ko and H. Song, *J. Mater. Chem.*, 2009, **20**, 1239-1246.
25. Y. Wang, J. Liu, P. Wang, C. J. Werth and T. J. Strathmann, *ACS Catal.*, 2014, **4**, 3551-3559.
26. J. Xu, Y.-Q. Deng, X.-M. Zhang, Y. Luo, W. Mao, X.-J. Yang, L. Ouyang, P. Tian and Y.-F. Han, *ACS Catal.*, 2014, **4**, 4106-4115.
27. E. Aneggi, D. Wiaters, C. d. Leitenburg, J. Llorca and A. Trovarelli, *ACS Catal.*, 2014, **4**, 172-181.
28. J. Li, Z. Zhang, Z. Tian, X. Zhou, Z. Zheng, Y. Ma and Y. Qu, *J. Mater. Chem. A*, 2014, **2**, 16459-16466.
29. S. Zhang, J. Li, W. Gao and Y. Qu, *Nanoscale* 2015, **7**, 3016-3021.
30. W. Tang, Z. Hu, M. Wang, G. D. Stucky, H. Metiu and E. W. McFarland, *J. Catal.*, 2010, **273**, 125-137.
31. A. P. Ferreira, D. Zanchet, J. C. S. Araújo, J. W. C. Liberatori, E. F. Souza-Aguiar, F. B. Noronha and J. M. C. Bueno, *J. Catal.*, 2009, **263**, 335-344.

Journal Name

32. L. Feng, D. T. Hoang, C.-K. Tsung, W. Huang, S. H.-Y. Lo, J. B. Wood, H. Wang, J. Tang and P. Yang, *Nano Research*, 2010, **4**, 61-71.
33. H. Mai, L. Sun, Y. Zhang, R. Si, W. Feng, H. Zhang, H. Liu and C. Yan, *J. Phys. Chem. B*, 2005, **109**, 24380-24385.
34. W. Gao, Z. Zhang, J. Li, Y. Ma and Y. Qu, *Nanoscale*, 2015, **7**, 11686-11691.
35. Y. Qu, A. M. Sutherland, J. Lien, G. D. Suarez and T. Guo, *J. Phys. Chem. Lett.*, 2010, **1**, 254-259.
36. H. Song, R. M. Rioux, J. D. Hoefelmeyer, R. Komor, K. Niesz, M. Grass, P. Yang and G. A. Somorjai, *J. Am. Chem. Soc.*, 2006, **128**, 3027-3037.
37. B. Li, T. Gu, T. Ming, J. Wang, P. Wang, J. Wang and J. C. Yu, *ACS Nano*, 2014, **8**, 8152-8162.
38. Z. Zhang, J. Li, W. Gao, Y. Ma and Y. Qu, *J. Mater. Chem. A*, 2015, **3**, 18074-18082.
39. M. Cargnello, J. J. Delgado Jaen, J. C. Hernandez Garrido, K. Bakhmutsky, T. Montini, J. J. Calvino Gamez, R. J. Gorte and P. Fornasiero, *Science*, 2012, **337**, 713-717.
40. Y. Zhu, S. Zhang, J.-j. Shan, L. Nguyen, S. Zhan, X. Gu and F. Tao, *ACS Catal.*, 2013, **3**, 2627-2639.
41. N. Zhang, X. Fu and Y.-J. Xu, *J. Mater. Chem.*, 2011, **21**, 8152-8158.
42. C. Zhang, S. Li, T. Wang, G. Wu, X. Ma and J. Gong, *Chem. Commun.*, 2013, **49**, 10647-10649.
43. L. Arroyo-Ramírez, C. Chen, M. Cargnello, C. B. Murray and R. J. Gorte, *Catal. Today*, 2015, **253**, 137-141.

Thermally stable sandwich-type catalysts of Pt nanoparticles encapsulated in CeO₂ nanorods/CeO₂ nanoparticles core/shell supports for methane oxidation at high temperatures

Zhiyun Zhang †, Jing Li †, Wei Gao, Zhaoming Xia, Yuanbin Qin, Yongquan Qu, Yuanyuan Ma *

Center for Applied Chemical Research, Frontier Institute of Science and Technology, and State Key Laboratory for Mechanical Behavior of Materials, Xi'an Jiaotong University, Xi'an, China, 710049. E-mail: yyma@mail.xjtu.edu.cn. Tel: +86-29-83395357.

A sandwich-type Pt nanocatalyst encapsulated ceria-based core-shell catalyst (CNR@Pt@CNP) was designed and synthesized, which exhibited high catalytic activity and remarkably thermal-stability at high temperatures up to 700 °C by effectively preventing the Pt nanocatalysts from thermal sintering and enhancing the metal-support interaction.

